The Journal of Neuroscience, December 1, 2001, 21(23):9403–9413

Voltage-Sensitive Dye Imaging of Neocortical Spatiotemporal Dynamics to Afferent Activation Frequency

Diego Contreras[1] **and Rodolfo Llinás**[2]

[1]*Department of Neuroscience, School of Medicine, University of Pennsylvania, Philadelphia, Pennsylvania 19104, and* [2]*Department of Physiology and Neuroscience, New York University School of Medicine, New York, New York 10016*

The spatial and temporal patterns of neocortex activation are determined not only by the dynamic character of the input but also by the intrinsic dynamics of the cortical circuitry. To study the role of afferent input frequency on cortical activation dynamics, the electrical activity of *in vitro* neocortex slices was imaged during white-matter electrical stimulation. High-speed optical imaging was implemented using voltage-sensitive dyes in guinea pig visual and somatosensory cortex slices concomitantly with intracellular recordings. Single white-matter electrical stimuli activated well-defined cortical sites with a radially oriented columnar configuration. This configuration was followed, over the next few milliseconds, by a lateral spread of excitation through cortical layers 5 and 6 and layers 2 and 3. Much of the optical response was eliminated in low extracellular calcium, indicating that it was primarily synaptically mediated.

Repetitive stimuli at 10 Hz reproduced the spatiotemporal pattern observed for single stimuli. In contrast, repetitive stimulation in the γ frequency range (~40 Hz) rapidly restrained the area of excitation to a small columnar site directly above the stimulating electrode. Intracellular recordings from cells lateral to the activated column revealed increased inhibitory synaptic activity and/or decreased excitatory responses during the train at 40 Hz, but not during a 10 Hz stimulation. Localized microinjections of $GABA_A$ antagonist produced a reorganization of the geometrical activity pattern that was dependent on the position of the microinjection site. These findings indicate that the frequency-dependent spatial organization of neocortex activation is determined by inhibitory sculpting attributable to local network dynamics.

Key words: optical; fluorescence; intracellular; cortex; voltage-sensitive dyes; γ; binding; 40 Hz

Neocortical network function has traditionally been assumed to be determined by the integrate and fire properties of local neurons and their connectivity (Calvin, 1975). In such models, spatiotemporal patterns of cortical activation depend solely on input dynamics and on the linear integrative properties of the target neurons. However, because neurons are endowed with nonlinear dynamic properties (Llinás, 1988) and synaptic strength is known to be activity modulated (Zucker, 1989), network dynamics cannot be defined solely on the basis of connectivity or single-stimulus activation.

One of the most dramatic examples of modulation of network dynamics occurs in thalamocortical networks with the transition from wakefulness to sleep. Thus, during slow-wave sleep (SWS) the spontaneous electroencephalogram (EEG) is dominated by high-amplitude, low-frequency oscillatory activity of <15 Hz showing long-range synchronization (Steriade et al., 1993b; Contreras et al., 1996, 1997). In contrast, during activated states (waking and paradoxical sleep), magnetoencephalographic (Ribary et al., 1991) and EEG activity are dominated by low-amplitude, high-frequency activity primarily at the γ frequency range (30–50 Hz) (Steriade et al., 1993b; Destexhe et al., 1999) and display restricted spatial synchrony (Ribary et al., 1991; Llinás and Ribary 1993; Steriade et al., 1996; Destexhe et al., 1999; Traub et al., 1999). It has been argued that spatially restricted fast oscillations are an essential step in the cortical processing of inputs because they allow the formation of groups of temporally coherent but spatially segregated clusters of neurons (Llinás and Pare, 1991; Llinás et al., 1998; Singer, 1999; Varela, 1999; see also Laurent, 1999). For this hypothesis to be viable, the existence of spatially independent oscillatory clusters regulated by thalamocortical resonance must be demonstrated. Such clusters should stabilize in a few re-entry cycles and must coexist in coherence with each other independently of cluster distance over the cortex, because the temporal binding would be implemented at the thalamic level (Llinás et al., 1998). Here we present evidence that the first of these prerequisites (i.e., the generation of spatially segregated fast oscillating cortical clusters) is obtainable by γ band afferent activation frequencies (~40 Hz).

A key factor that could play a major role in shaping the cortical activation geometry to afferent input frequency is the action of local inhibitory neurons (Kawaguchi and Kubota 1993; Cauli et al., 1997; DeFelipe, 1999; Gibson et al., 1999; Gupta et al., 2000). Indeed, GABAergic inhibition has been shown to be critical in the stability of cortical function, because its selective block induces epilepsy (Prince, 1968; Connors, 1984; Steriade and Contreras, 1998; McCormick and Contreras, 2001). Moreover, a subpopulation of layer 4 inhibitory interneurons exhibits intrinsic oscillatory activity in the γ frequency band (Llinás et al., 1991). When local circuit synapses are compared, excitatory connections into GABAergic interneurons exhibit a more rapid and profound frequency-dependent depression (Thomson and Deuchars, 1997;

Received June 26, 2001; revised Sept. 18, 2001; accepted Sept. 18, 2001.

This work was supported by the Human Frontier Science Organization, by the Research Foundation of the University of Pennsylvania, and by National Institutes of Health/National Institute of Neurological Disorders and Stroke Grant NS13742. We thank Joseph Frey for his technical assistance and Elena Leznik and Francisco Urbano for their help in experiments and analysis.

Correspondence should be addressed to R. Llinás, Department of Physiology and Neuroscience, New York University School of Medicine, 550 First Avenue, New York, NY 10016. E-mail: Llinar01@endeavor.med.nyu.edu.

 0270-6474/01/219403-11$15.00/0

Galarreta and Hestrin, 1998) than do the inhibitory outputs of those interneurons. In addition, it has been shown recently that the output of interneurons with low-threshold spike (LTS) firing characteristics onto spiny stellate cells facilitates strongly when activated at 40 Hz, but not when activated at 10 Hz (Gibson et al., 1999). Such interneurons are interconnected by chemical and electrical junctions (Gibson et al., 1999). Because of all of the characteristics mentioned above, it is reasonable to suggest that the spatiotemporal properties of cortical responses to sustained input at fast frequencies could in fact be shaped primarily by inhibitory circuits.

MATERIALS AND METHODS

Slice preparation and staining. Adult guinea pigs were deeply anesthetized with sodium pentobarbital (50 mg/kg, i.p.) and decapitated after loss of limb-withdrawal reflex. Brains were removed and transferred to chilled (4°C) Krebs–Ringer's solution containing (in mM): 126 NaCl, 5 KCl, 2 $CaCl_2$, 13 $MgSO_4$, 12 KH_2PO_4, 26 $NaHCO_3$, and 10 glucose saturated with a mixture of 95% O_2 and 5% CO_2. In the experiments in which no Ca^{2+} solution was used, magnesium was increased by 2 mM, but calcium chelators were not included. Coronal and sagittal slices (400 μm thick) were prepared from the visual and somatosensory cortex using a vibratome. Slices were stained with the voltage-sensitive dye RH795 (Molecular Probes, Eugene, OR) (Grinvald et al., 1994) dissolved (0.5 mg/ml) in normal Krebs–Ringer's medium with 0.5% of dimethylsulfoxide. Slices were submerged for 4–5 min in the dye solution before being transferred to the recording chamber. Recordings were made in an interface-type chamber at 35 ± 0.5°C. Handling and care of experimental animals was in agreement with the policy established by New York University Medical Center and by the American Physiological Society.

Optical recordings. A schematic drawing of the recording set-up is shown in Figure 1*A*. An upright microscope (Olympus BX50WI; Olympus Optical, Tokyo, Japan) was mounted on an X-Y table (Warner Instruments, Hamden, CT), with the recording chamber and micromanipulators attached to a rigid stand. Epi-illumination was provided by a halogen lamp (12 V) driven by a stable power supply (Kepco, Flushing, NY). Optical signals were monitored with a fast CCD camera (HRDeltaron 1700; Fujix, Tokyo, Japan) with a 128 × 128 pixel matrix and a total frame speed of 0.6 msec (Matsumoto and Ichikawa, 1990). Although in a few instances the area imaged was 8.2 × 8.2 mm, the imaged area was 4.3 × 4.3 mm for the majority of the experiments, such that each pixel collected light from a small region of 34 × 34 μm. The optical data sets represent averages of either 8 or 16 trains of stimulation. Fluorescence values are differential because each frame represents the difference between the signal generated in response to stimulation minus the value of a reference frame, multiplied by 400. A reference frame was calculated as the average of 64 frames (0.6 msec integration time) preceding the stimulation train. Stimuli (1–5 V, 100 μsec) were applied by means of bipolar electrodes to the underlying white matter.

To determine whether the change in the amplitude of the fluorescence signal ΔF was significantly different from fractional fluorescence, $\Delta F/F$ (Grinvald et al., 1982), fractional fluorescence was determined in a set of experiments ($n = 5$). As illustrated in Figure 1*B*, the activation spatiotemporal patterns was virtually identical with both methods. Because the absolute fluorescence value is not relevant in this study and because our aim was to investigate the patterns of cortical activation, only ΔF was used in the rest of the figures.

Intracellular recordings and electrical stimulation. Cells were recorded intracellularly using sharp micropipettes (tip resistances of between 40 and 80 MΩ filled with 3 M potassium acetate). Electrodes were advanced blindly using a hydraulic microdrive. Recordings were made using a bridge amplifier (Cygnus Technology, Delaware Water Gap, PA) and were digitized at 10 kHz using an analog-to-digital board (GW Instruments, Somerville, MA) into a PC computer for offline analysis. Analysis of intracellular data was done with home-written routines using an Igor package (WaveMetrics Inc., Lake Oswego, OR).

Electrical stimulation was delivered by concentric bipolar electrodes (platinum–iridium wire; 25 μm inner pole; 200 μm outer pole) (model CBBRC75; Frederick Haer Co., Bowdoinham, ME) gently placed over the surface of the white matter. Stimulation consisted of 100 μsec pulses at 0.5–2 mA delivered through stimulus isolation units (World Precision Instruments, Sarasota, FL).

Data analysis. Bleaching and irregularities of the staining, although not significant, were corrected off-line by normalizing the imaged surface. Signals were smoothed with a three-dimensional (3-D) moving average of 3 × 3 × 3 points and with equal weight to eliminate high-frequency noise. All optical data analyses were performed with software written in Matlab (Mathworks Inc., Natick, MA).

Histological controls. Some slices ($n = 4$) were fixated in formaldehyde (4%), resectioned, and stained with cresyl violet to identify cortical layers.

RESULTS

Our database was obtained from 31 experiments. Coronal or sagittal slices (400 μm thick) from the visual ($n = 24$) and somatosensory ($n = 9$) cortex were used. The responses to single and repetitive stimuli were similar for both orientations and brain regions studied; therefore, they will be presented together. Slices were stained with the voltage-sensitive dye RH795 (Molecular Probes) and electrical stimuli (100 μsec; 0.5–2 mA) were delivered to the subcortical white matter. Optical images were recorded with a fast (1700 frames/sec) CCD camera (HRDeltaron) and intracellular recordings ($n = 26$) were obtained from layers 2–6 using sharp micropipettes (40–80 MΩ impedance). Only those intracellular recordings having resting membrane potentials negative to −70 mV, stable for >15 min, and with input resistances of >20 MΩ were considered in the database.

Comparison of optical signals with intracellular voltage

The first set of experiments compared the time course and amplitude of the voltage-sensitive dye signals with simultaneously obtained intracellular voltage recordings. With the voltage-sensitive dye RH795, membrane depolarization is accompanied by a decrease in fluorescence (Grinvald et al., 1994), represented here as a positive signal. Simultaneous intracellular and optical recordings ($n = 12$) indicated a close correlation between the two types of signals (Fig. 1*C*) (Tanifuji et al., 1994; Antic et al., 1999). In a representative case illustrated in Figure 1*C*, the intracellular response matched closely the fluorescence signal of the recording site (position 2, indicating the recording micropipette location). To analyze the ionic origin of the voltage response, we imposed transmembrane potential (V_m) changes in the recorded cell using current-clamp DC injections. Membrane depolarization revealed that the initial depolarization was attributable to a short-lasting EPSP followed by a reversed biphasic IPSP.

These IPSPs had a reversal potential (E_{IPSP}) of −73 mV and so were reversed at the resting potential (−77 mV). The matching of the intracellular and optical data (Fig. 1*C*) was always best at resting V_m, indicating that the V_m of the recorded cell was indeed representative of the population generating the optical signal. The mean resting V_m ($n = 26$) was −78 ± 5 mV, which is negative to the E_{IPSP} and partially explains why the majority of the optical images indicated depolarizing responses.

Because a certain decree of phototoxicity is expected from voltage-sensitive dye activation (Momose-Sato et al., 1995), we tested cell viability by determining changes in excitability using current-pulse injections (Fig. 1*D*). Depolarizing pulses of increasing amplitudes were used to evaluate the frequency response properties of the cell and to measure action potential characteristics. Such pulses produced results that concurred with the firing characteristics described previously in cortical cells *in vitro* (Connors et al., 1982; McCormick et al., 1985) and *in vivo* (Nunez et al., 1993) indicating no evidence of cytotoxicity. In addition, input resistance was monitored using hyperpolarizing current pulses. Such measurements were done repeatedly during the recording of optical responses. The stability of the responses over time indi-

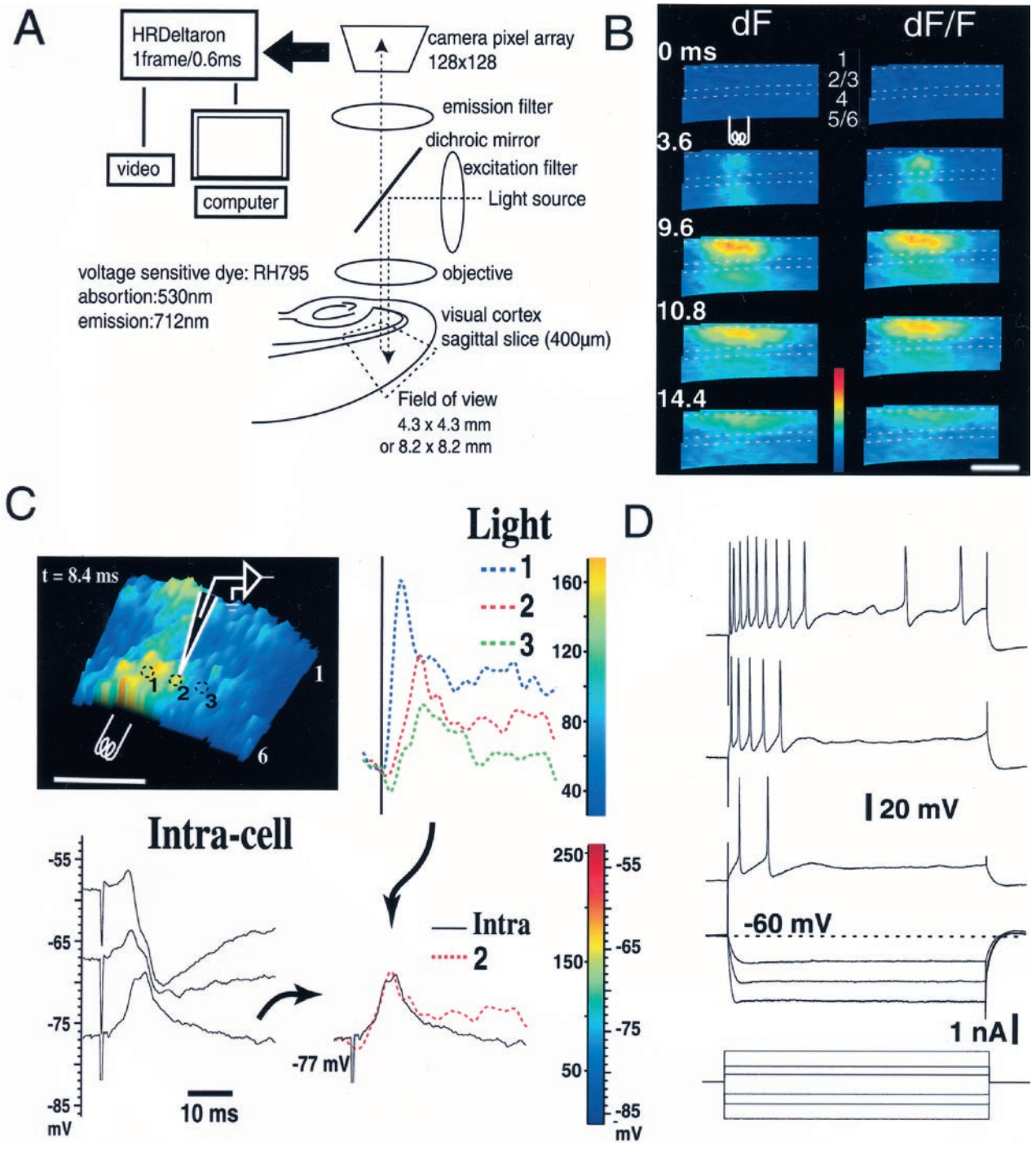

Figure 1. *A*, Scheme of the setup arrangement for optical recordings. The size of the field of view as well as filter settings and wavelengths are indicated. *B*, Snapshots of the response to a single electrical stimulus applied to the white matter (guinea pig visual cortex slice) and recorded using differential fluorescence (*df*) (*left*) and $\Delta F/F$ (*right*). The responses were almost identical. The color scale from *blue* to *red* represents a 0–0.48% change in $\Delta F/F$ and a 0–255 change in df. Layers are indicated and are based on Nissl-stained sections. *C*, Comparison of fluorescence values with intracellular membrane potential. Fluorescence (recorded as df) and membrane potential (V_m) in response to a single stimulus to the white matter are shown. *Top left*, A snapshot of activity (layers and stimulating electrode position are indicated) at 8.4 msec after the stimulus was applied to the white matter; *circles* represent three arbitrary points where pixel values were obtained. Intracellular recording was from position 2, as indicated by the pipette. *Top right*, Time course and amplitude of fluorescence values obtained at points 1–3. *Bottom left*, Synaptic responses at three different V_ms to single stimuli applied to the white matter. *Bottom right*, A comparison of the time course and amplitudes of light and of a cell at rest (−77 mV) recorded from position 3. *D*, Depopolarizing and hyperpolarizing pulses applied to the same cell as in *C* at various times during the recording to verify that input resistance and action potential characteristics are unaltered and the slice is healthy. The cell depicted is a regular spiking cell from upper layer 6, with an input resistance of 39 MΩ. Scale bar: *B, C*, 1 mm.

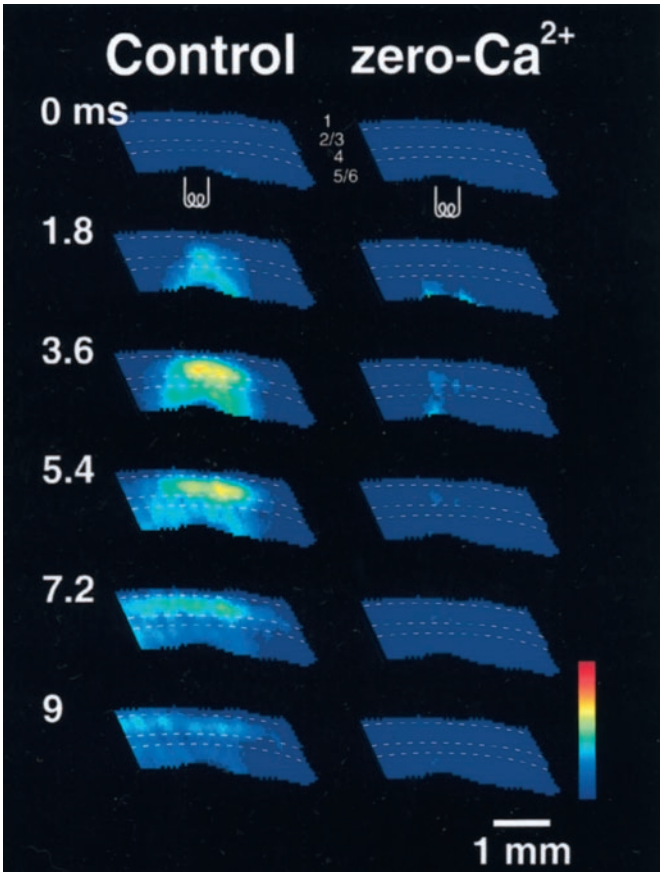

Figure 2. Optical recordings are primarily generated by orthodromic activation. Snapshots of the optical responses to a single stimulus under control conditions (*left*) show that the response was almost completely abolished after 30 min of perfusion in a medium in which Ca^{2+} was substituted with Mg^{2+} (*right*). Cortical layers and the position of stimulating electrodes are indicated.

cated no obvious tissue damage imposed by our experimental procedure.

Optical responses were primarily generated by synaptic activation

Electrical stimulation of the white matter underlying the cortical mantle excites both cortical afferent (primarily consisting of corticocortical and thalamocortical fibers) and efferent fibers. Thus, optical responses may result from antidromic or orthodromic (monosynaptic and/or polysynaptic) activation. However, on occasion such electrical stimuli may also directly activate cells in layer 6 and the basal dendrites of layer 5 cells.

To separate the synaptic and nonsynaptic (antidromic and direct) contribution to the optical responses, we perfused the slice in medium in which extracellular Ca^{2+} was substituted with Mg^{2+} (4 mM; $n = 5$) (Fig. 2) for a period of 30–40 min before stimulation. Under this condition, most of the optical response was eliminated, except for focal activation in layer 6 and in layers 2 and 3 in the vertical axis above the stimulating electrode with no horizontal displacement. Activation of layers 2 and 3 was observed 1.8 msec after activation of layer 6. Indeed, vertical propagation with the Ca^{2+}-free medium occurred at velocities similar to those seen for the control images.

We attributed the activation of layers 2 and 3 in the absence of Ca^{2+} to antidromic invasion, because those layers project to neighboring cortical regions and are the origin of the callosal connectivity (Miller, 1975; Swadlow and Weyand, 1981; Segraves and Rosenquist, 1982). A contributing factor may also be dendritic backpropagation from layer 5 and layer 6 pyramidal neurons (Stuart et al., 1997), although it is not known how much backpropagation may occur based solely on dendritic Na^+ currents (Huguenard et al., 1989; Schwindt and Crill, 1997), and most of the apical dendrite excitability after somatic action potentials seems to be attributable to Ca^{2+} electrogenesis (Yuste et al., 1994; Helmchen et al., 1999; Svoboda et al., 1999).

Response to single stimuli

The optical response to a single white-matter stimulus (Fig. 3*A*, see also Fig. 1*B* for comparison with fractional fluorescence) was characterized in both visual ($n = 24$) and somatosensory ($n = 9$) cortical slices. Frequently the response consisted of an initial layer 6 activation immediately above the electrode (frame at 1.2 msec). This event was followed by a propagation of activation toward layer 1 and a close to simultaneous horizontal activation through layers 6 and 5 (see frame at 2.4 msec). After reaching layers 2 and 3, the activation propagated horizontally through those layers as well (frame at 3.6 msec and after), albeit more slowly than through deep layers. Responses were always larger in the deep (5 and 6) and superficial (2 and 3) layers than in layer 4 (see for example frame at 6.0 msec), with maximum amplitude in layers 2 and 3.

To measure the extent and the velocity of the propagation in different directions and planes, we constructed activation profiles (Fig. 3*B*). These images represent fluorescence signal against time from those pixels that fall under an arbitrary line drawn over the slice image. Three activation profiles are represented in Figure 3*B*: one vertical (from layers 1–6, *bottom left*) and two horizontal (layers 2 and 3, *top right*; layers 5 and 6, *bottom right*). The horizontal activation profiles were traced left to right as indicated in Figure 3, *right*. Because activation profiles represent space against time, the velocity of propagation is given by the slope of the apparent activation front (defined as the visible separation between activated and nonactivated areas). If the velocity is uniform, the activation front is close to a straight line, which is the case for the propagation toward the left of the slice in deep and superficial layers. If propagation velocity were to be site-specific, then the apparent activation front in the profile would show slope changes. Because space is represented on the *x*-axis and time on the *y*-axis, an increase or decrease in slope corresponds to a decrease or increase in propagation velocity. Nonhomogeneous propagation fronts can be seen in both horizontal profiles in Figure 3*B* when activation moves from the center toward the right side of the slice.

To detect heterogeneities in the spatial and/or temporal distribution of fluorescence, we integrated pixel values in the activation profiles against time (overlying white lines in the profiles). This procedure demonstrated that activation is not uniform in the vertical direction. Indeed, as discussed above, infragranular and supragranular layers showed larger activation than layer 4, with a maximum in layers 2 and 3. In contrast, horizontal activation profiles showed evenly distributed activation with a bilaterally smooth decay from the center of the slice, where the stimulating electrode was located. In most experiments ($n = 12$), activation propagated vertically from layers 6–1 at 265 ± 48 mm/sec (mean ± SD) and horizontally through deep layers at 217 ± 53 mm/sec. Propagation through layers 2 and 3 occurred at 181 ± 44 mm/sec. In some cases, profiles such as those illustrated in Figure

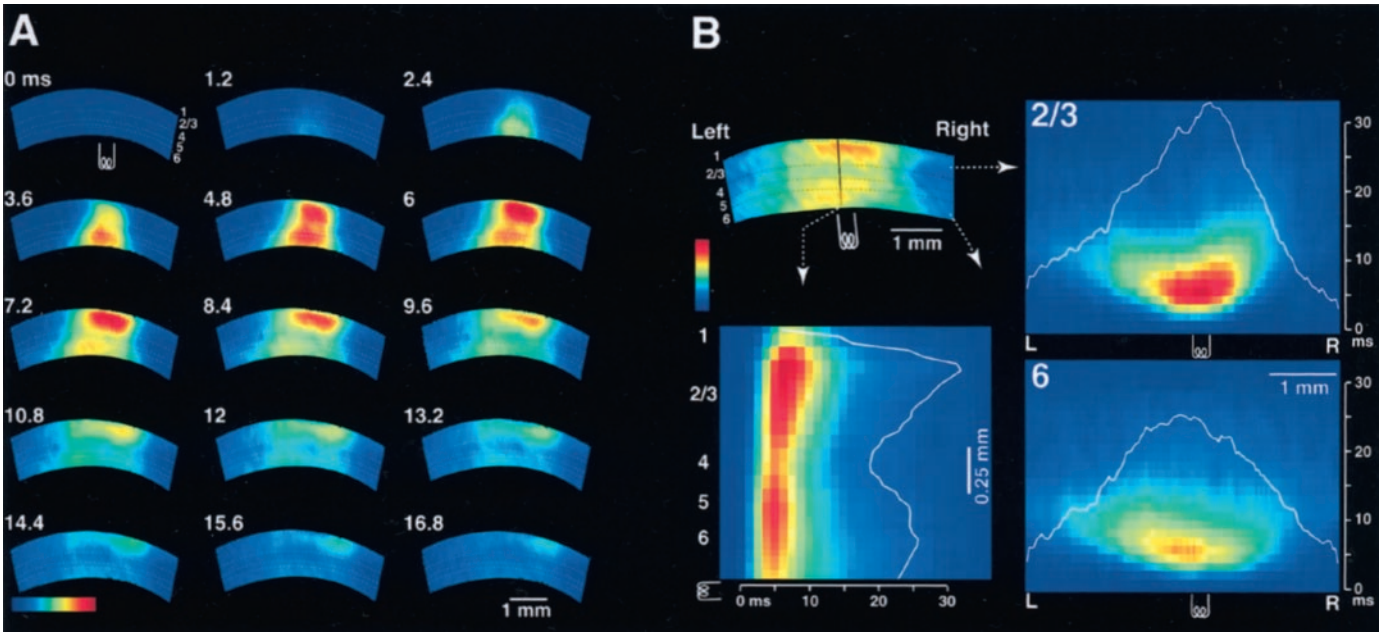

Figure 3. *A*, Spatiotemporal patterns of activation resulting from electrical stimulation of the white matter. Optical recordings from guinea pig visual cortex are shown. Time is indicated in milliseconds after the stimulus, and the position of the stimulating electrode is indicated as well. The cortex is positioned with layer 1 on the *top* and layer 6 on the *bottom*. The color scale for fluorescence intensity is arbitrary between 0 (*blue*) and 255 (*red*). *B*, Activation profiles after a single electrical stimulus was applied to the white matter. A visual cortex slice is shown. *Top left*, A snapshot of activation at $t = 8.4$ msec; layers are indicated. *Bottom left*, Temporal evolution (*x*-axis) of activation along a *vertical line* from layers 1–6 (*y*-axis). The *overlying white line* is the summation of pixel values across time (from *left* to *right*) and shows maxima in layers 2 and 3 with a second peak in infragranular layers. *Right*, Temporal evolution of the activity along a line of pixels parallel to the pial surface within layers 2 and 3 (*top*) and layer 6 (*bottom*). Space is represented from *left* (*L*) to *right* (*R*) of the slice (*x*-axis); time after stimulation is indicated on the *y*-axis. Profiles show not only the extent and velocity of propagation but also the duration of the activation of any given pixel.

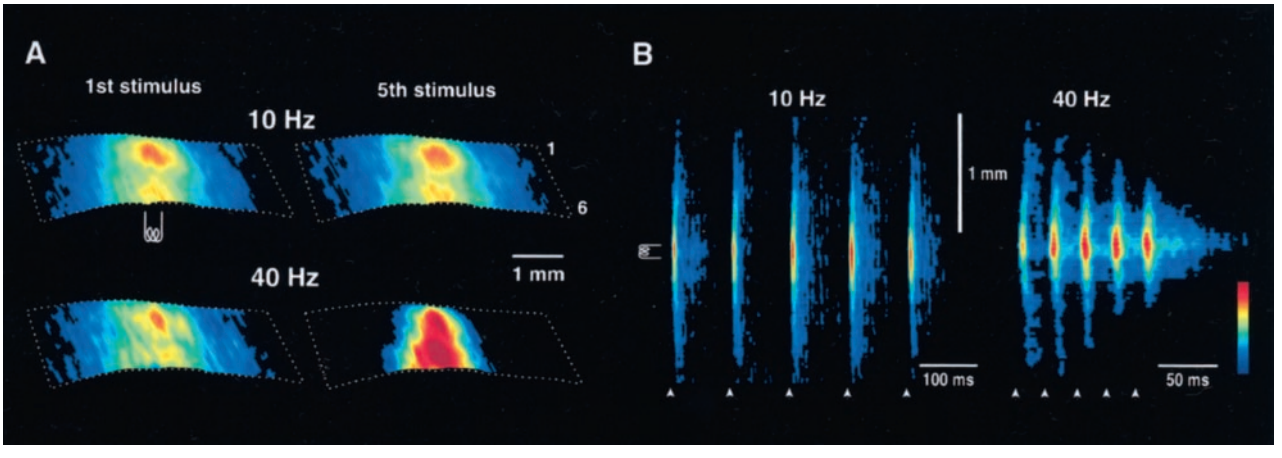

Figure 4. *A*, Spatiotemporal characteristics of activation depend on the frequency of stimulation. Snapshots at 7.2 msec after stimulation during the first (*left*) and fifth (*right*) stimuli during trains at 10 (*top row*) and 40 Hz (*bottom row*) are shown. The color code for intensity ranges from 0 to 255. Responses to the first stimulus were identical at both frequencies. The response to the fifth stimulus did not change when stimulation was at 10 Hz; in contrast, the activation area became smaller and the response amplitude became higher during stimulation at 40 Hz. *B*, Temporal evolution of the spatiotemporal properties of activation during repetitive stimulation (*arrowheads*). Activation profile (as in Fig. 3*B*) across layers 2 and 3 in a visual cortical slice. Distance is indicated on the *y*-axis, and time is indicated on the *x*-axis. Activation spanned the entire length (~2.2 mm) of the profile for each stimulus at 10 Hz but shrunk progressively to ~1 mm during stimulation at 40 Hz.

3*B* indicate asymmetric activation in the horizontal plane. We attributed these asymmetries to slice section characteristics, because on some occasions slices demonstrated symmetrical activation profiles (Fig. 4). The horizontal extent of propagation measured from the activation profiles after single stimuli was 2.1 ± 0.4 mm in each direction from the stimulating electrode; the extent of propagation was similar among slices, regardless of cortical orientation and brain region.

Response to rhythmic input activation

The dependence of the activation pattern on white-matter stimulation frequency was explored with two different frequencies, 10 and 40 Hz. These frequencies were chosen to mimic the prevailing rhythms present *in vivo* during SWS and activated states, respectively (see the introductory remarks). During trains of stimulation at 10 Hz, activation patterns extended laterally over a

large portion of the slice and remained constant throughout the train. The extent and the velocity of propagation showed almost no change, such that the first and fifth stimulus in a train produced similar optical images (Fig. 4*A*, 10 Hz). In contrast, stimulation at 40 Hz progressively reduced the activation area to a vertical column-like geometry that overlaid the stimulating electrode (Fig. 4*A*, 40 Hz). The average area of activation after repetitive stimulation at 40 Hz extended laterally for <0.5 mm and showed higher peak amplitude than during the 10 Hz stimulation. On occasion, such activity could be as wide as 1 mm, depending on stimulus intensity (see Fig. 7 below).

The dynamics of the optical responses in the horizontal plane after different activation frequencies are best illustrated by plotting activation profiles (Fig. 4*B*). The activation profile depicted in Figure 4*B* represents fluorescence along layers 2 and 3 in response to stimulation of the white matter. With stimulation at 10 Hz (Fig. 4*B*, *left*), the optical response after each stimulus spanned the entire length of the tissue (~2 mm) for each response. At 40 Hz (Fig. 4*B*, *right*), a progressive decrease in the lateral extent of the activation was observed to ~1 mm after the fifth stimulus. There was also a marked increase in the amplitude of the optical signal in the center of the activated area. This was demonstrative of a powerful and localized temporal summation during the 40 Hz frequency stimulation.

Spatial interaction between two cortical activation sites

In light of the results shown above, we expected, as briefly reported previously (Llinás et al., 1998), that responses should coalesce spatially when stimulation at 10 Hz is applied at more than one site, whereas stimulation at ~40 Hz should give rise to segregated response areas. The dynamics of the responses to more than one stimulation site were studied by stimulating the white matter with two electrodes separated by 1–4 mm. In the example shown in Figure 5, two stimulating electrodes were placed in the white matter separated by 1.5 mm; trains of 10 stimuli at 10 Hz (Fig. 5, *top*) and 40 Hz (Fig. 5, *bottom*) were applied, first with each of the electrodes individually (*Electrode 1* and *Electrode 2*) and then with both simultaneously (*Both*). The response depicted in Figure 5 is to the 10th stimulus. Stimulation with each of the electrodes alone (Fig. 5, *left* and *middle*) gave rise to responses with the spatiotemporal pattern described above, namely, responses to the 40 Hz train evolved toward a spatially restricted and high-amplitude pattern, whereas responses at 10 Hz remained stable and spread laterally. When stimulation was delivered through both electrodes simultaneously (Fig. 5, *Both*), the responses to 10 Hz propagated horizontally and collided in the middle of the slice. In contrast, the responses to the 40 Hz stimulation developed into two segregated areas with high amplitude and separated by a region with no optical signal.

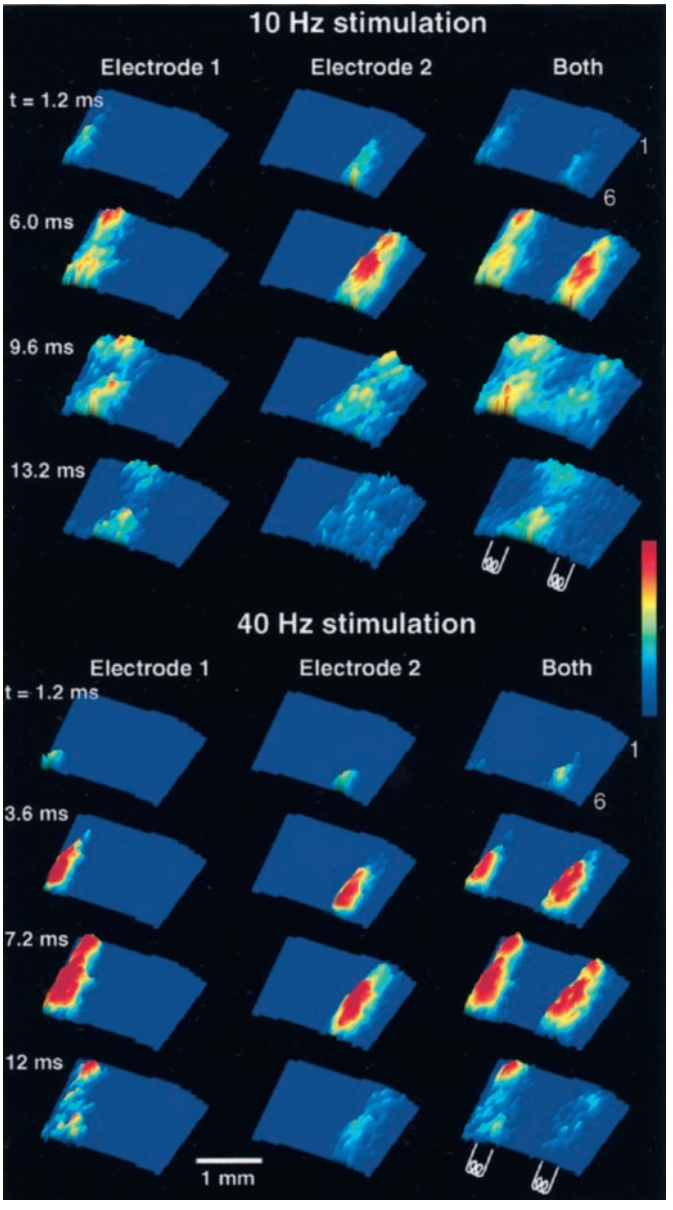

Figure 5. Spatiotemporal aspects of activation with two electrodes. A slice from the visual cortex was stimulated with two electrodes in the white matter separated by 1.5 mm. The 3-D snapshots illustrate the evolution of the optical response for the 10th stimulus in a train at 10 Hz (*top*) and 40 Hz (*bottom*). The responses to the 10th stimulus delivered by each electrode and then the two simultaneously are illustrated. During stimulation at 40 Hz, the activated areas remain segregated. The position of stimulating electrode is indicated.

Intracellular responses to repetitive stimulation

The cellular mechanisms underlying the optical responses described above were investigated by comparing fluorescence signals with intracellular recordings. Two sites were investigated (Fig. 6): one immediately above the stimulating electrode (*dotted lines*, area 1) and one equidistant from both electrodes (area 2). During the 10 Hz stimulation (Fig. 6, *LIGHT*; 10 Hz), fluorescence signals remained almost unchanged in amplitude and duration at both sites, with values from site 2 having smaller amplitudes, slower rising phases, and longer latencies (~2 or 3 msec) than values from site 1. In contrast, during stimulation at 40 Hz (Fig. 6, *LIGHT*; 40 Hz), pixel values did not remain constant; in site 1 there was strong temporal summation and in site 2 there was a progressive decrease in amplitude. Variations in the amplitude of the responses during the 40 Hz stimulation were only attributable to the frequency of the stimulation, because the first response for trains at both frequencies was virtually identical (see superimposition of first and last responses at the *bottom right* of Fig. 6).

Intracellular recordings obtained from the same two areas (Fig. 6, V_m) showed results that were similar to those observed for the fluorescence signals. Stimulation at 10 Hz (Fig. 6, *A1*) generated depolarizing PSPs that did not change in amplitude or duration

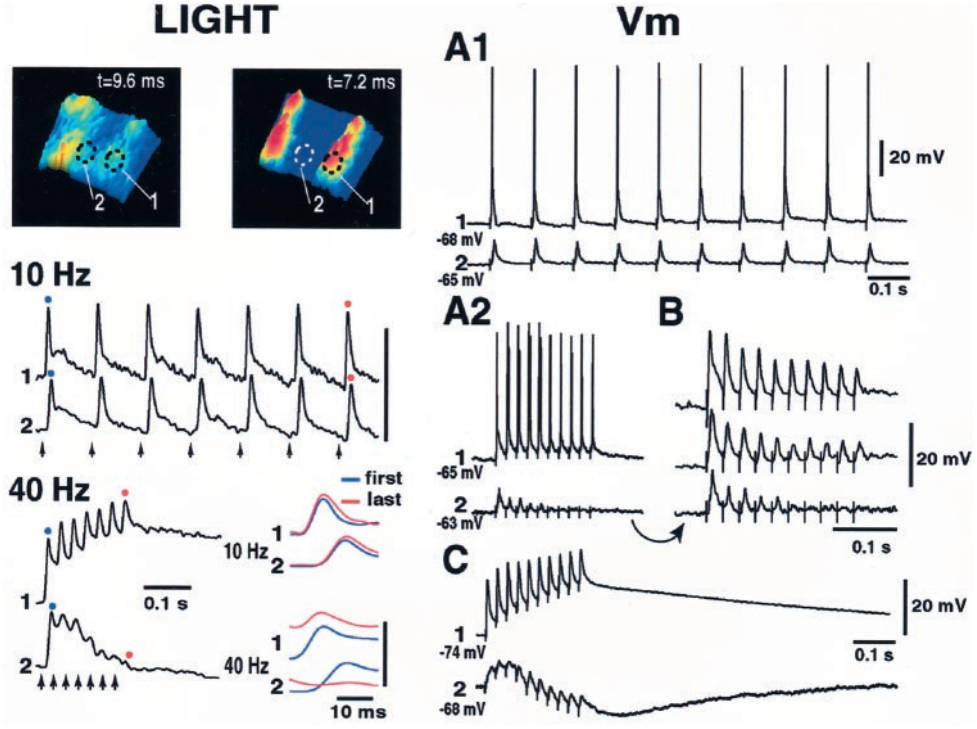

Figure 6. Pixel values and intracellular recordings during stimulation at different frequencies. Fluorescence values (*LIGHT*) and intracellular recordings (V_m) were obtained from areas 1 and 2 (*dotted lines*) during stimulation at 10 and 40 Hz (*A1* and *A2*, respectively, in V_m). *Bottom right*, Comparisons of the first (*blue dot*) and the last (*red dot*) of the responses during the trains at the two frequencies are superimposed. *B*, Cell from position 2 in *A2* (*arrow*). Increasing the intensity of stimulation (from bottom up) triggered responses to all stimuli at 40 Hz. *C*, Different cells showing long-lasting inhibition triggered by a 40 Hz stimulation.

with respect to the first response in cells recorded from both area 1 and area 2. PSPs from the cell in area 2 showed a latency that was similar to that seen for the fluorescence signal. Stimulation at 40 Hz generated synaptic responses in cells from area 1 showing different degrees of temporal summation (Fig. 6, *A2* and *C*). We recorded two types of synaptic responses from cells in area 2: (1) a marked depression of the synaptic response (Fig. 6, *A2*) ($n = 7$) usually between stimuli 4 and 7, or (2) a clear EPSP in response to each stimulus but on a background of a growing IPSP triggered during the train (Fig. 6*C*) ($n = 3$). The difference did not depend on layer, electrophysiological cell type, or intensity of stimulation. Additional experiments are necessary to clarify this issue.

Increasing the intensity of stimulation at 40 Hz led to the generation of responses in the cells recorded from site 2 for all of the stimuli in the train (Fig. 6*B*, V_m). This was accompanied by the generation of a corresponding optical signal at site 2 which, as shown above, had no optical signal at a lower intensity of stimulation after 4 or 5 stimuli (data not shown). We attributed this effect to an increase in the activated area because of stimulus current spread. This is indeed equivalent to bringing the stimulating electrode closer to site 2, thus converting the stimulus geometry similar to site 1. However, a similar increase in stimulation intensity only increased the amplitude of the IPSP for those cells that responded with inhibition, suggesting that there is more than simply the recruitment of more afferent axons by current spread.

The drastic reduction of synaptic amplitude during stimulation at 40 Hz was further analyzed by holding the cell at different V_ms during the stimulus train (Fig. 7) ($n = 5$). Stimulation at rest (Fig. 7*A*, −78 mV) elicited depolarizing PSPs exclusively, which showed a marked depression during the train (Fig. 7*C*). DC depolarization to −53 mV (Fig. 7*A–C*, *top traces*) revealed that the response to the first stimulus consisted of a short EPSP with a peak latency of 5 msec; this EPSP was sharply terminated by a fast IPSP with a peak latency of 9.5 msec and a reversal potential of −72 mV. The reversal potential and short duration suggest that the IPSP was caused by the activation of $GABA_A$ receptors. At more positive V_ms, the synaptic response to the last few stimuli of the train was almost completely abolished; however, a depolarizing response could still be recorded with hyperpolarization. This result indicated that the depression of the synaptic response occurred at the expense of the early EPSP. To verify this possibility, we scaled the amplitude of the response to the last stimulus with the response to the first stimulus and superimposed the two (Fig. 7*D*). The superimposition showed that the response to the last stimulus lacked the initial EPSP, reinforcing the notion that the depression observed in site 2 during stimulation at 40 Hz is primarily attributable to EPSP depression, which suggests a reduction of a polysynaptic circuit or a very powerful synaptic shunt, probably at a remote dendritic level.

The response to a single stimulus showed an early EPSP followed by a biphasic IPSP, probably attributable to the activation of $GABA_A$ and $GABA_B$ receptors, as has been described *in vitro* (Connors et al., 1988). The presence of a long-lasting IPSP modulating the responses to the train could be seen by superimposing a single stimulus to the train responses (Fig. 7*E*).

Inhibition shapes spatiotemporal properties of evoked responses

Finally, we blocked $GABA_A$ receptors with bicuculline to test the role played by GABAergic inhibition in shaping the spatiotemporal activation patterns described above. Two methodologies were used: bath application by superfusion ($n = 6$) and local application ($n = 12$) of bicuculline through a micropipette inserted into the slice parenchyma. After perfusion, a single stimulus caused an epileptogenic high-amplitude wave that propagated primarily through layers 2 and 3 and layers 5 and 6, across the entire slice at ~0.1–0.3 mm/sec, similar to that described using field potentials (Connors, 1984). In contrast, local application did not alter the normal response to stimulation, except for

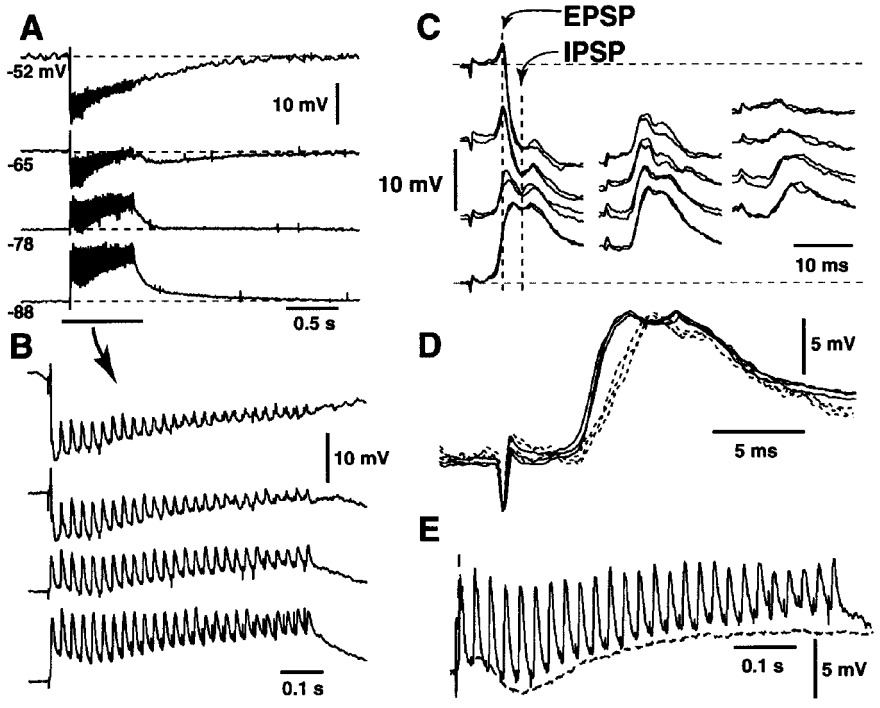

Figure 7. Membrane polarization reveals frequency-dependent depression of EPSP. A cell recorded intracellularly from the column above the stimulating electrode is shown. *A*, Electrical stimulation at 40 Hz was delivered to the white matter while changing the V_m of the cell with DC. *Traces* are displaced artificially for clarity. V_m is indicated. *B*, Detail of the responses from *A*, as indicated by the *black bar*. *C*, Detail from the first, middle, and last synaptic responses from trains in *A* and *B*. *Vertical dotted lines* indicate the peak of the EPSP and IPSP, respectively. *Horizontal dotted lines* are the most depolarized and hyperpolarized V_ms because of DC injection. *D*, Superimposition of the first and last responses (*dotted line*, scaled to match amplitude of the first response). The last response lacks the EPSP and consists almost exclusively of an inverted IPSP. *E*, Comparison of the train of responses with response to a single stimulus; the time course of the response to a single shock matches the underlying shape of the train.

an expansion of the activation boundary at the site of the injection (Fig. 8, *Control*). Indeed, when stimuli were delivered to the immediate vicinity of the injection site, activation occurred in a localized but almost explosive manner and had a long time course (hundreds of milliseconds) such that the usual dynamic properties of the cortical activation were obliterated. When the injection of bicuculline was made at the boundary of the area that responds in control conditions after a single stimulus, it produced an extension of the response to the single stimulus into the injection site (Fig. 8, site *b*); this response showed a large amplitude and persisted for 200–300 msec (Fig. 8, *Bic position 1*, *red line* in plot). Finally, an injection was placed in a site beyond the observable limit of the control activation wave (Fig. 8, site *c*). Activation after a single stimulus proceeded as in the control but eventually invaded the injection area, although this site was noncontiguous with the control activation region (Fig. 8, *Bic position 2*, *green line* in plot).

DISCUSSION

The main thrust of this work was aimed at understanding the dynamics of cortical activation in response to different input frequencies. Our results show that the cortical spatiotemporal activation patterns, after stimulation of the underlying white matter, are critically determined by the stimulus frequency. We also show that cortical activation patterns are partially dependent on local $GABA_A$ gated inhibition. In addition, the results were independent of orientation of the slice plane or brain region. Therefore, we concluded that the cortical spatiotemporal patterns described here must reflect a general property of at least primary sensory regions of the neocortex.

The origin of the optical signal

Most of the optical signal from the neocortex recorded using voltage-sensitive dyes originates from dendrites of pyramidal and spiny stellate cells (Grinvald et al., 1994; Yuste et al., 1997). An additional source of the optical signal is the depolarization of non-neuronal elements such as glial cells during repetitive stimulation (Konnerth et al., 1987; Salzberg, 1989). A possible explanation for the lower amplitude of signals in layer 4 reported here is the presence of strong local inhibition activated by layer 6 input (Bolz and Gilbert, 1986). This assumption is corroborated by the finding that adding bicuculline increased the amplitude of layer 4 activation (Fig. 8).

The advantage of voltage-sensitive dye imaging over field potentials or current-source density analysis is that V_m is recorded directly and simultaneously from a large number of cells. Other publications have elegantly addressed the differences between local field potentials and optical signals (Salzberg et al., 1973; Albowitz and Kuhnt, 1993a).

Horizontal propagation

Our results show propagation patterns in agreement with previous voltage-dependent dye measurements from the visual (Albowitz and Kuhnt, 1993a; Tanifuji et al., 1994; Nelson and Katz, 1995) and auditory (Kubota et al., 1997) cortices and with the detailed analysis of the visual cortex microcircuitry using voltage-sensitive dyes (Yuste et al., 1997). In contrast, our experiments measured activity over a broader field of view and revealed lateral activation of 2 mm in each direction, more than double that found in previous studies for the visual cortex (Tanifuji et al., 1994; Nelson and Katz, 1995) or the auditory cortex (Kubota et al., 1997).

Our measurements of horizontal conduction velocities show higher values than those reported by others (Tanifuji et al., 1994), probably because we did not use bicuculline in our control experiments. Bicuculline enhances the optical signal but generates a significant reduction of propagation velocities and changes the distribution of activity in horizontal propagation (Nelson and Katz, 1995) (our unpublished observations). Indeed, we expect the velocities to increase during cortical activation, such as occurs under the influence of neuromodulation (McCormick, 1992), a situation in which neurons are depolarized and thus closer to firing threshold.

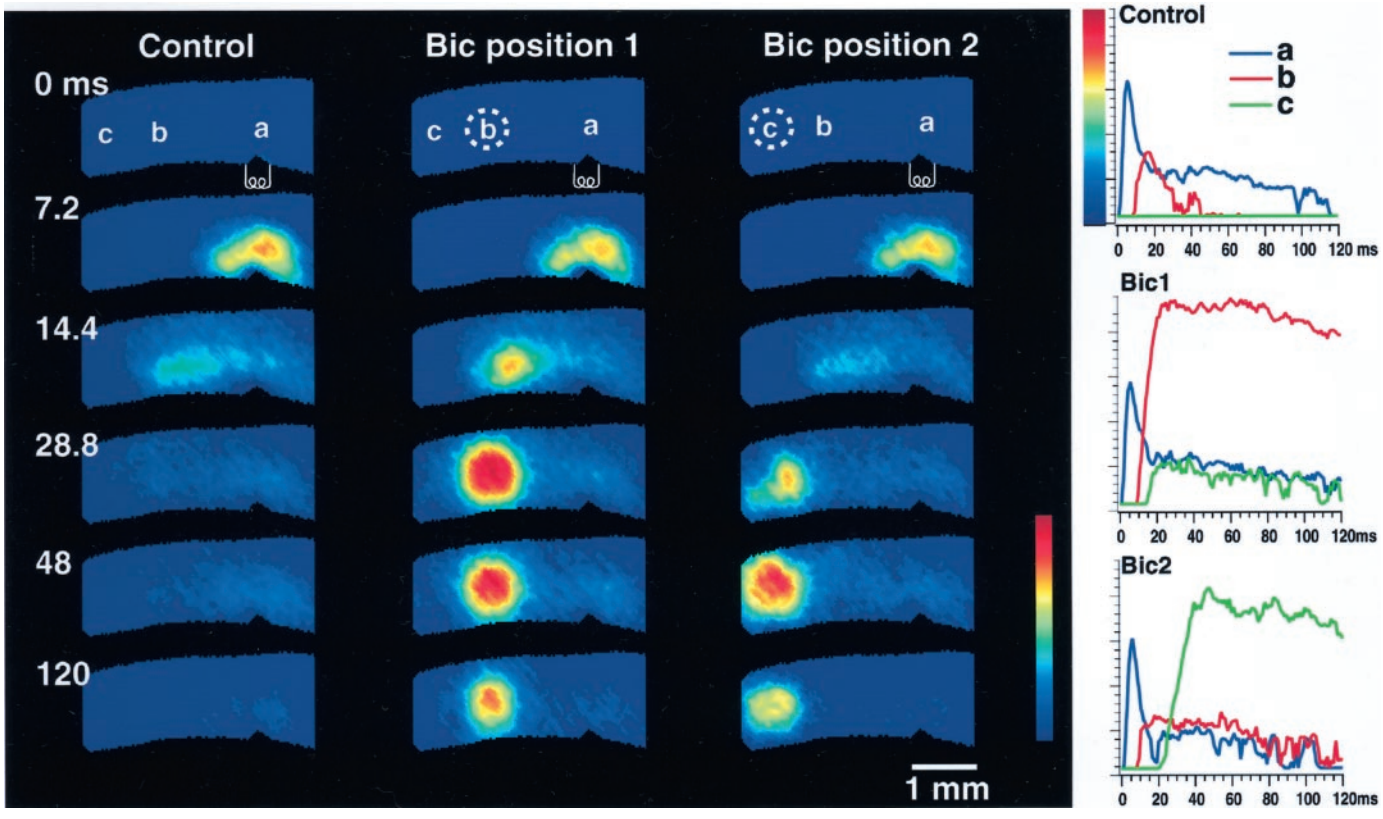

Figure 8. Spatiotemporal properties of activation after a single stimulus were altered by local injection of bicuculline. *Left*, Snapshots of the control response to a single stimulus applied to the white matter; time after stimulus is indicated on the *left*. *Middle*, Pattern of propagation after local injection of bicuculline (*dotted circle*) in position *b*. *Right*, Pattern of propagation after local injection of bicuculline (*dotted circle*) in position *c*. Values from pixels located in positions *a* (*blue*), *b* (*red*), and *c* (*green*) along the path of propagation are plotted on the *right*. Note that the pixel values are plotted against the 0–255 color scale represented on the *left*. Activation invaded areas farther away from the stimulation site according to the location of the bicuculline injection.

Propagation of activity in the horizontal direction may be attributable to (1) divergent translaminar connections or (2) horizontal intralaminar connections. Divergent translaminar projections originate from all cortical layers and terminate preferentially in layers 2 and 3 (Fitzpatrick et al., 1996; Somogyi et al., 1998). Horizontal intralaminar projections are most prominent in layers 2 and 3 and are absent in layer 4 (Gilbert 1992; Fitzpatrick et al., 1996; Somogyi et al., 1998). Alternatively, activity may propagate through regenerative loops using both vertical interlaminar connections and horizontal intralaminar projections (Tanifuji et al., 1994). Our data do not allow discrimination between the different alternatives, but because propagation velocities in the vertical and horizontal directions were of the same order of magnitude, it seems unlikely that the horizontal propagation that we measured was attributable to complex regenerative circuits.

Antidromic versus orthodromic activation: the synaptic origin of the optical signal

Comparison of the fluorescence responses to V_m recorded intracellularly showed that the optical recordings primarily reflect synaptically derived potentials ranging from 5 to 20 mV in amplitude and very little contribution of action potentials. This finding is in agreement with previous reports (Albowitz and Kuhnt 1993a,b; Tanifuji et al., 1994; Cohen and Yarom, 2000). Our results showed that in the absence of extracellular calcium, most of the optical response is absent. The remaining fluorescence (Fig. 2) consisted of a brief optical signal originating in layer 6 followed by layers 2 and 3. This low Ca^{2+} response may be attributable to (1) orthodromic activation of presynaptic terminals of corticocortical or thalamocortical afferents or (2) antidromic activation neurons in layers 2–6 in conjunction with some degree of dendritic backpropagation of the action potential (Stuart et al., 1997). We favor the second alternative because: (1) The results show absence of lateral spread both in superficial and deep layers and absence of layer 4 activity. This finding also excludes a presynaptic origin because thalamocortical presynaptic terminals should be visible in layer 4. In addition, the neurons in layers 5 and 6 and layers 2 and 3 have axon collaterals with abundant lateral spread inconsistent with the spatially restricted signal shown here. (2) The slow time course of the response (>3 msec to reach layers 2 and 3) is consistent with some contribution of dendritic backpropagation from layers 5 and 6. Given the absence of Ca^{2+} in the bath, the contribution of backpropagation to the response would be supported by the different types of Na^+ conductances present in the apical dendrites (Huguenard et al., 1989; Schwindt and Crill, 1997).

Role of inhibition on the geometry of cortical activation

Our experimental design was also aimed at determining the contribution of GABA-mediated inhibition to the geometry of cortical activation. $GABA_A$ blockers (such as bicuculline) have been shown to increase both the optical response amplitude as

well as the area of cortical activation after a single stimulus (Albowitz and Kuhnt, 1993a,b; Tanifuji et al., 1994). However, in those studies bicuculline was applied to the bath, blocking inhibition throughout the entire slice; therefore, the propagating excitation was abnormally large in extent and amplitude. Here we applied bicuculline at restricted small areas in the depth of the cortical tissue, which did not interfere with normal propagation in the rest of the slice. Our results show that synaptic activation after application of a single stimulus to the white matter reaches beyond the area observed by the optical signals. Such activity is not visible in control conditions probably because of powerful local inhibition that restricts local excitatory re-entry. In support of this interpretation, we found that the GABA antagonist injection sites placed beyond the outer edge of the optical response were eventually invaded by activity and that, as expected, such activation had the long-delay characteristic of polysynaptic re-entry loops (Fig. 8, *right*).

Our results also suggest that although inhibition is important in the normal distribution of cortical activation, it plays a crucial role in the geometry of the γ band activation pattern. Indeed it seems to be the basic sculpting mechanism for γ band activation (Llinás, 1990), as suggested by the intrinsic oscillatory properties of the sparsely spiny GABAergic interneurons in layers 3 and 4 (Llinás et al., 1991). Those cells were shown to have oscillatory intrinsic activity supported by persistent sodium conductances that could be blocked by tetrodotoxin (Llinás et al., 1991). In addition, it has been shown recently (Gibson et al., 1999) that activation of a particular set of inhibitory interneurons (LTS neurons) is strongly potentiated for input frequencies at ~40 Hz, which suggests that this type of interneuron may play an important role in the frequency-dependent geometry of cortical activation.

Input frequency determines spatiotemporal pattern of cortical activation

The finding that repetitive stimulation may alter the dynamic architecture of cortical activation indicates that frequency has intrinsic significance in cortical function. In agreement with recent findings showing that thalamic neurons can also oscillate at γ frequency (Contreras et al., 1992; Pinault and Deschenes, 1992; Steriade et al., 1993a; Pedroarena and Llinás, 1997), it was proposed that γ oscillations result in the generation of spatially restricted thalamocortical oscillatory columns by resonant thalamocortical activity (Llinás, 1990; Llinás et al., 1991, 1998; Ribary et al., 1991; Pedroarena and Llinás, 1997). Our results show that restricted, discrete regions of activation of cortex, as observed *in vivo*, may be obtained by activation at γ band frequencies. Because we could obtain such patterns with nonspecific stimulation of the white matter in slices, it is reasonable to suppose that the spatiotemporal differences observed *in vivo* are attributable, at least in part, to a fundamental property of cortical circuits.

The columnar organization of thalamocortical γ band activity

It has been known since the groundbreaking experiments of Mountcastle (1957) and Hubel and Wiesel (1962) that physiological cortical responses demonstrate columnar organization. Cortical columns (300–600 μm in diameter) are defined functionally by the grouping of neurons with similar properties and were first described in the somatosensory cortex of the cat and monkey (Mountcastle, 1957; Powell and Mountcastle, 1959). Columnar organization is maintained by the characteristics of afferent inflow and by the subsequent intracortical processing; the relative importance of each in shaping cortical columns varies with cortical area (Mountcastle, 1997). The anatomical basis for columnar organization is the clustered nature of thalamocortical input (Jones, 1983) and the local intracortical connections in the vertical axis (Lorente de No, 1938; Szentagothai, 1975), which engage neurons in all layers during activation. Cortical columns may be regarded as modules for distributed coherent information processing and, if so, their functional isolation would be fundamental in neocortical functioning. We have shown here that γ band frequency is critical in determining the formation of patches of activation that resemble cortical columns, although the areas reported here are of slightly larger diameter (up to 1 mm).

In summary, the central finding in this study relates to the presence of separable clusters of cortical activity that are defined by the dynamics of the afferent input frequency, in particular by γ band activity. This clustering seems to be independent of neighboring structures and to be operant in a horizontally isotropic manner (Fig. 5). Given that spatial focusing of cortical activation during a 40 Hz stimulation can occur after just a few stimuli, such spatial filtering could be established very rapidly in an *in vivo* situation. We may imagine a scenario in which corticothalamic network activity at the γ band could support the varied and ever-changing activity necessary for the generation of consciousness in the vertebrate brain (Llinás et al., 1998).

REFERENCES

Albowitz B, Kuhnt U (1993a) Evoked changes of membrane potential in guinea pig sensory neocortical slices: an analysis with voltage-sensitive dyes and a fast optical recording method. Exp Brain Res 93:213–225.

Albowitz B, Kuhnt U (1993b) Spread of epileptiform potentials in the neocortical slice: recordings with voltage-sensitive dyes. Brain Res 631:329–333.

Antic S, Major G, Zecevic D (1999) Fast optical recordings of membrane potential changes from dendrites of pyramidal neurons. J Neurophysiol 82:1615–1621.

Bolz J, Gilbert CD (1986) Generation of end-inhibition in the visual cortex via interlaminar connections. Nature 320:362–365.

Calvin WH (1975) Generation of spike trains in CNS neurons. Brain Res 84:1–22.

Cauli B, Audinat E, Lambolez B, Angulo MC, Ropert N, Tsuzuki K, Hestrin S, Rossier J (1997) Molecular and physiological diversity of cortical nonpyramidal cells. J Neurosci 17:3894–3906.

Cohen D, Yarom Y (2000) Cerebellar on-beam and lateral inhibition: two functionally distinct circuits. J Neurophysiol 83:1932–1940.

Connors BW (1984) Initiation of synchronized neuronal bursting in neocortex. Nature 310:685–687.

Connors BW, Gutnick MJ, Prince DA (1982) Electrophysiological properties of neocortical neurons in vitro. J Neurophysiol 48:1302–1320.

Connors BW, Malenka RC, Silva LR (1988) Two inhibitory postsynaptic potentials and $GABA_A$ and $GABA_B$ receptor-mediated responses in neocortex of rat and cat. J Physiol (Lond) 406:443–468.

Contreras D, Curro Dossi R, Steriade M (1992) Bursting and tonic discharges in two classes of reticular thalamic neurons. J Neurophysiol 68:973–977.

Contreras D, Destexhe A, Sejnowski TJ, Steriade M (1996) Control of spatiotemporal coherence of a thalamic oscillation by corticothalamic feedback. Science 274:771–774.

Contreras D, Destexhe A, Sejnowski TJ, Steriade M (1997) Spatiotemporal patterns of spindle oscillations in cortex and thalamus. J Neurosci 17:1179–1196.

DeFelipe J (1999) Chandelier cells and epilepsy. Brain 122:1807–1822.

Destexhe A, Contreras D, Steriade M (1999) Spatiotemporal analysis of local field potentials and unit discharges in cat cerebral cortex during natural wake and sleep states. J Neurosci 19:4595–4608.

Fitzpatrick D (1996) The functional organization of local circuits in visual cortex: insights from the study of tree shrew striate cortex. Cereb Cortex 6:329–341.

Galarreta M, Hestrin S (1998) Frequency-dependent synaptic depression and the balance of excitation and inhibition in the neocortex. Nat Neurosci 1:587–594.

Gibson JR, Beierlein M, Connors BW (1999) Two networks of electrically coupled inhibitory neurons in neocortex. Nature 402:75–79.

Gilbert CD (1992) Horizontal integration and cortical dynamics. Neuron 9:1–13.

Grinvald A, Hildesheim R, Farber IC, Anglister L (1982) Improved fluorescent probes for the measurement of rapid changes in membrane potential. Biophys J 39:301–308.
Grinvald A, Lieke EE, Frostig RD, Hildesheim R (1994) Cortical point-spread function and long-range lateral interactions revealed by real-time optical imaging of macaque monkey primary visual cortex. J Neurosci 14:2545–2568.
Gupta A, Wang Y, Markram H (2000) Organizing principles for a diversity of GABAergic interneurons and synapses in the neocortex. Science 287:244–246.
Helmchen F, Svoboda K, Denk W, Tank DW (1999) In vivo dendritic calcium dynamics in deep-layer cortical pyramidal neurons. Nat Neurosci 2:989–996.
Hubel DH, Wiesel TN (1962) Receptive fields, binocular interaction, and functional architecture in the cat's visual cortex. J Physiol (Lond) 160:106–154.
Huguenard JR, Hamill OP, Prince DA (1989) Sodium channels in dendrites of rat cortical pyramidal neurons. Proc Natl Acad Sci USA 86:2473–2477.
Jones EG (1983) The nature of the afferent pathways conveying short-latency inputs to primate motor cortex. Adv Neurol 39:263–285.
Kawaguchi Y, Kubota Y (1993) Correlation of physiological subgroupings of nonpyramidal cells with parvalbumin- and calbindinD28k-immunoreactive neurons in layer V of rat frontal cortex. J Neurophysiol 70:387–396.
Konnerth A, Obaid AL, Salzberg BM (1987) Optical recording of electrical activity from parallel fibres and other cell types in skate cerebellar slices *in vitro*. J Physiol (Lond) 393:681–702.
Kubota M, Sugimoto S, Horikawa J, Nasu M, Taniguchi I (1997) Optical imaging of dynamic horizontal spread of excitation in rat auditory cortex slices. Neurosci Lett 237:77–80.
Laurent G (1999) A systems perspective on early olfactory coding. Science 286:723–728.
Llinás R (1988) The intrinsic electrophysiological properties of mammalian neurons: insights into central nervous system function. Science 242:1654–1664.
Llinás R (1990) Intrinsic electrical properties of mammalian neurons and CNS function. In: Fidia Research Foundation Neuroscience Award Lectures (Changeux J-P, Llinás R, Purves D, Bloom FE, eds), pp 175–194. New York: Raven.
Llinás R, Pare D (1991) Of dreaming and wakefulness. Neuroscience 44:521–535.
Llinás R, Ribary U (1993) Coherent 40-Hz oscillation characterizes dream state in humans. Proc Natl Acad Sci USA 90:2078–2081.
Llinás R, Grace AA, Yarom Y (1991) *In vitro* neurons in mammalian cortical layer 4 exhibit intrinsic oscillatory activity in the 10- to 50-Hz frequency range. Proc Natl Acad Sci USA 88:897–901.
Llinás R, Ribary U, Contreras D, Pedroarena C (1998) The neuronal basis for consciousness. Philos Trans R Soc Lond B Biol Sci 353:1841–1849.
Lorente de No R (1938) Cerebral cortex: architecture, intracortical connections, motor projections. In: Physiology of the nervous system (Fulton J, ed), pp 288–338. Oxford: Oxford UP.
Matsumoto G, Ichikawa M (1990) Optical system for real-time imaging of electrical activity with a 128 × 128 photopixel array. Soc Neurosci Abstr 16:490.
McCormick DA (1992) Neurotransmitter actions in the thalamus and cerebral cortex. J Clin Neurophysiol 9:212–223.
McCormick DA, Contreras D (2001) On the cellular and network bases of epileptic seizures. Annu Rev Physiol 63:815–846.
McCormick DA, Connors BW, Lighthall JW, Prince DA (1985) Comparative electrophysiology of pyramidal and sparsely spiny stellate neurons of the neocortex. J Neurophysiol 54:782–806.
Miller R (1975) Distribution and properties of commissural and other neurons in cat sensorimotor cortex. J Comp Neurol 164:361–373.
Momose-Sato Y, Sato K, Sakai T, Hirota A, Matsutani K, Kamino K (1995) Evaluation of optimal voltage-sensitive dyes for optical monitoring of embryonic neural activity. J Membr Biol 144:167–176.
Mountcastle VB (1957) Modality and topographic properties of single neurons of cat's somatic sensory cortex. J Neurophysiol 20:408–434.
Mountcastle VB (1997) The columnar organization of the neocortex. Brain 120:701–722.
Nelson DA, Katz LC (1995) Emergence of functional circuits in ferret visual cortex visualized by optical imaging. Neuron 15:23–34.
Nunez A, Amzica F, Steriade M (1993) Electrophysiology of cat association cortical cells in vivo: intrinsic properties and synaptic responses. J Neurophysiol 70:418–430.
Pedroarena C, Llinás R (1997) Dendritic calcium conductances generate high-frequency oscillation in thalamocortical neurons. Proc Natl Acad Sci USA 94:724–728.
Pinault D, Deschenes M (1992) Voltage-dependent 40-Hz oscillations in rat reticular thalamic neurons *in vivo*. Neuroscience 51:245–258.
Powell T, Mountcastle V (1959) Some aspects of the functional organization of the cortex of the postcentral gyrus of the monkey: a correlation of findings obtained in a single unit analysis with cytoarchitecture. Bull Johns Hopkins Hosp 105:133–162.
Prince DA (1968) Inhibition in local epileptogenesis. Electroencephalogr Clin Neurophysiol 24:290–293.
Ribary U, Ioannides AA, Singh KD, Hasson R, Bolton JP, Lado F, Mogilner A, Llinás R (1991) Magnetic field tomography of coherent thalamocortical 40-Hz oscillations in humans. Proc Natl Acad Sci USA 88:11037–11041.
Salzberg BM (1989) Optical recording of voltage changes in nerve terminals and in fine neuronal processes. Annu Rev Physiol 51:507–526.
Salzberg BM, Davila HV, Cohen LB (1973) Optical recording of impulses in individual neurones of an invertebrate central nervous system. Nature 246:508–509.
Schwindt PC, Crill WE (1997) Local and propagated dendritic action potentials evoked by glutamate iontophoresis on rat neocortical pyramidal neurons. J Neurophysiol 77:2466–2483.
Segraves MA, Rosenquist AC (1982) The distribution of the cells of origin of callosal projections in cat visual cortex. J Neurosci 2:1079–1089.
Singer W (1999) Neuronal synchrony: a versatile code for the definition of relations? Neuron 24:49–65, 111–125.
Somogyi P, Tamas G, Lujan R, Buhl EH (1998) Salient features of synaptic organisation in the cerebral cortex. Brain Res Brain Res Rev 26:113–135.
Steriade M, Contreras D (1998) Spike-wave complexes and fast components of cortically generated seizures. I. Role of neocortex and thalamus. J Neurophysiol 80:1439–1455.
Steriade M, Curro Dossi R, Contreras D (1993a) Electrophysiological properties of intralaminar thalamocortical cells discharging rhythmic (approximately 40 Hz) spike-bursts at approximately 1000 Hz during waking and rapid eye movement sleep. Neuroscience 56:1–9.
Steriade M, McCormick DA, Sejnowski TJ (1993b) Thalamocortical oscillations in the sleeping and aroused brain. Science 262:679–685.
Steriade M, Contreras D, Amzica F, Timofeev I (1996) Synchronization of fast (30–40 Hz) spontaneous oscillations in intrathalamic and thalamocortical networks. J Neurosci 16:2788–2808.
Stuart G, Spruston N, Sakmann B, Hausser M (1997) Action potential initiation and backpropagation in neurons of the mammalian CNS. Trends Neurosci 20:125–131.
Svoboda K, Helmchen F, Denk W, Tank DW (1999) Spread of dendritic excitation in layer 2/3 pyramidal neurons in rat barrel cortex in vivo. Nat Neurosci 2:65–73.
Swadlow HA, Weyand TG (1981) Efferent systems of the rabbit visual cortex: laminar distribution of the cells of origin, axonal conduction velocities, and identification of axonal branches. J Comp Neurol 203:799–822.
Szentagothai J (1975) The "module-concept" in cerebral cortex architecture. Brain Res 95:475–496.
Tanifuji M, Sugiyama T, Murase K (1994) Horizontal propagation of excitation in rat visual cortical slices revealed by optical imaging. Science 266:1057–1059.
Thomson AM, Deuchars J (1997) Synaptic interactions in neocortical local circuits: dual intracellular recordings in vitro. Cereb Cortex 7:510–522.
Traub RD, Whittington MA, Buhl EH, Jefferys JG, Faulkner HJ (1999) On the mechanism of the $\gamma \rightarrow \beta$ frequency shift in neuronal oscillations induced in rat hippocampal slices by tetanic stimulation. J Neurosci 19:1088–1105.
Varela FJ (1999) Cognition without representations. Riv Biol 92:511–512.
Yuste R, Gutnick MJ, Saar D, Delaney KR, Tank DW (1994) Ca^{2+} accumulations in dendrites of neocortical pyramidal neurons: an apical band and evidence for two functional compartments. Neuron 13:23–43.
Yuste R, Tank DW, Kleinfeld D (1997) Functional study of the rat cortical microcircuitry with voltage-sensitive dye imaging of neocortical slices. Cereb Cortex 7:546–558.
Zucker RS (1989) Short-term synaptic plasticity. Annu Rev Neurosci 12:13–31.